JGR Space Physics

RESEARCH ARTICLE
10.1029/2020JA027823

Special Section:
Early results from the Global-scale Observations of the Limb and Disk (GOLD) mission

Initial Observations by the GOLD Mission

R. W. Eastes[1], W. E. McClintock[1], A. G. Burns[2], D. N. Anderson[3], L. Andersson[1], S. Aryal[1], S. A. Budzien[4], X. Cai[2], M. V. Codrescu[3], J. T. Correira[5], R. E. Daniell[6], K. F. Dymond[4], S. L. England[7], F. G. Eparvier[1], J. S. Evans[5], H. Foroosh[8], Q. Gan[1], K. R. Greer[1], D. K. Karan[1], A. Krywonos[9], F. I. Laskar[1], J. D. Lumpe[10], C. R. Martinis[11], J. B. McPhate[12], J. Oberheide[13], O. H. Siegmund[12], S. C. Solomon[2], V. Veibel[5], and T. N. Woods[1]

[1]Laboratory for Atmospheric and Space Physics, University of Colorado Boulder, Boulder, CO, USA, [2]High Altitude Observatory, National Center for Atmospheric Research, Boulder, CO, USA, [3]NOAA-SEC and CIRES, University of Colorado Boulder, Boulder, CO, USA, [4]Naval Research Laboratory, Washington, DC, USA, [5]Computational Physics Inc., Springfield, VA, USA, [6]Ionospheric Physics, Stoughton, MA, USA, [7]Aerospace and Ocean Engineering, Virginia Polytechnic Institute and State University, Blacksburg, VA, USA, [8]Computer Science, University of Central Florida, Orlando, FL, USA, [9]Florida Space Institute, University of Central Florida, Orlando, FL, USA, [10]Computational Physics Inc., Boulder, CO, USA, [11]Center for Space Physics, Boston University, Boston, MA, USA, [12]Space Science Lab, University of California, Berkeley, CA, USA, [13]Physics and Astronomy, Clemson University, Clemson, SC, USA

Key Points:
- GOLD makes global-scale, synoptic measurements of the temperature, composition, and densities in the thermosphere-ionosphere system
- Most measurements by the GOLD instrument are made in one of four modes
- The observations are providing new and surprising insights into the characteristics and behavior of the thermosphere and ionosphere

Correspondence to:
R. W. Eastes,
richard.eastes@lasp.colorado.edu

Citation:
Eastes, R. W., McClintock, W. E., Burns, A. G., Anderson, D. N., Andersson, L., Aryal, S., et al. (2020). Initial observations by the GOLD mission. *Journal of Geophysical Research: Space Physics*, *125*, e2020JA027823. https://doi.org/10.1029/2020JA027823

Received 21 JAN 2020
Accepted 18 MAY 2020
Accepted article online 23 MAY 2020

Abstract The NASA Global-scale Observations of the Limb and Disk (GOLD) mission has flown an ultraviolet-imaging spectrograph on SES-14, a communications satellite in geostationary orbit at 47.5°W longitude. That instrument observes the Earth's far ultraviolet (FUV) airglow at ~134–162 nm using two identical channels. The observations performed include limb scans, stellar occultations, and images of the sunlit and nightside disk from 6:10 to 00:40 universal time each day. Initial analyses reveal interesting and unexpected results as well as the potential for further studies of the Earth's thermosphere-ionosphere system and its responses to solar-geomagnetic forcing and atmospheric dynamics. Thermospheric composition ratios for major constituents, O and N_2, temperatures near 160 km, and exospheric temperatures are retrieved from the daytime observations. Molecular oxygen (O_2) densities are measured using stellar occultations. At night, emission from radiative recombination in the ionospheric *F* region is used to quantify ionospheric density variations in the equatorial ionization anomaly (EIA). Regions of depleted *F* region electron density are frequently evident, even during the current solar minimum. These depletions are caused by the "plasma fountain effect" and are associated with the instabilities, scintillations, or "spread *F*" seen in other types of observations, and GOLD makes unique observations for their study.

Plain Language Summary The NASA Global-scale Observations of the Limb and Disk (GOLD) mission has flown a dual-channel, ultraviolet-imaging spectrograph on SES-14, a communications satellite in geostationary orbit at 47.5°W longitude. That instrument observes the Earth's far ultraviolet (FUV) airglow at ~134–162 nm. The observations performed include images of the Earth's sunlit and nightside disk, limb scans, and stellar occultations, from 6:10 to 00:40 universal time each day. Initial analyses reveal interesting and unexpected results as well as the potential for further studies of the Earth's thermosphere-ionosphere system and its responses to solar-geomagnetic forcing and atmospheric dynamics. Thermospheric temperatures and composition ratios for major constituents, O and N_2, near 160-km altitude and exospheric temperatures are retrieved from the daytime observations. Molecular oxygen (O_2) densities are measured using stellar occultations. At night, emission from radiative recombination in the ionospheric *F* region is used to quantify ionospheric density variations in the equatorial ionization anomaly (EIA). Regions of depleted *F* region electron density are frequently evident in the EIA, even during the current solar minimum.

1. Introduction

The GOLD mission provides unprecedented imaging of the Earth's space environment, enabling the upper atmosphere to be viewed as a space weather system. The instrument is a dual-channel, spectral imager hosted in geostationary orbit on SES-14, a commercial communications satellite located at 47.5°W longitude. From there, the imager observes the Far Ultraviolet (FUV) spectrum of the Earth's atmosphere. GOLD is a

National Aeronautics and Space Administration (NASA) mission of opportunity that was launched into geostationary transfer orbit on 25 January 2018 by an Ariane 5 vehicle. Electric propulsion was employed to raise perigee and circularize the orbit, and the satellite achieved geostationary orbit in July 2018. Instrument checkout was performed during September 2018, and routine observations commenced on 9 October 2018.

From GOLD's spectral images, simultaneous images of thermospheric temperature and neutral composition ratios ($\Sigma O/N_2$, column density ratio) are derived at a half-hour cadence during daytime full-disk observations. Daytime limb observations, made following most daytime disk scans, are used to derive exospheric temperatures. At night, GOLD images the low-latitude ionosphere where regions of depleted density caused by instabilities or irregularities that form after dusk are frequently observed. Molecular oxygen (O_2) density profiles, rather than a limb scan within the half-hour, are obtained at all local times (LTs) from stellar occultations.

The value of $\Sigma O/N_2$ observations has been demonstrated by the Global Ultraviolet Imager (GUVI) instrument on the NASA TIMED (Thermosphere Ionosphere Mesosphere Energy and Dynamics) satellite. Those data have revolutionized our understanding of the thermosphere-ionosphere (T-I) system, providing new insights into its state and response to forcing. The GOLD imager also measures $\Sigma O/N_2$ but from the perspective of geostationary orbit, allowing it to separate temporal and spatial changes over the Americas and Atlantic. GOLD can observe the entire disk at a 30-min cadence. In addition to $\Sigma O/N_2$ GOLD also provides simultaneous images of neutral temperatures from the same altitudes, near 160 km.

2. GOLD Instrument

Each identical, independent channel of GOLD imager observes the full ~134- to 162-nm spectrum. Each also has a scan mirror and an imaging detector. The imaging detector provides spectral information at spatial locations along the entrance slit. Three-dimensional (3-D) spatial-spectral image cubes are constructed by combining observations taken while the entrance slit scans across the desired area, for example, the limb or the entire disk of the Earth. Disk images covering ~$\pm$70° in latitude and longitude relative to spacecraft nadir, as well as the Earth's limb to >600-km tangent altitude, can be obtained. In the following discussions, the two channels are referred to as A and B, with A being the one located more inboard. From each, the location and pulse heights of individual photon detection events are downlinked at a 0.1-s cadence; spatial-spectral binning and all subsequent processing are done on the ground. Each channel also has three entrance slits. The narrowest, ~0.2 nm, high-resolution slit is used for limb and dayside disk observations. An example of the spectrum obtained using that slit is shown in Figure 1. The low-resolution, ~0.35 nm, slit is used for night observations, and the widest, ~2.3 nm, is used for stellar occultations. Instrument details can be found in Eastes et al. (2017).

3. Observations

During GOLD's normal operations, it typically cycles through four specific modes based on time of day and the opportunities for observations. While the capabilities of the instrument allow dramatic changes to the observing schedule and modes, almost all of the observations have been and continue to be a full-disk scan, limb scan, partial-disk scan, or occultation. Each of the two channels follows independent observation schedules. A small portion of the observations use “special” modes which utilize the flexibility and independence of the channels to perform observations in which the instrument's operation is tailored to the objectives. Examples include the partial-disk scans conducted during the July 2019 eclipse (Aryal et al., 2019) and those made in search of gravity wave signatures in the lower-middle thermosphere that were reported by England et al. (2020).

Only minor changes have been made in the observing schedule since regular operations began in October 2018. During routine daily operations, each channel initially observed the Earth from 03:00 to 21:00 LT (06:10 to 00:10 universal time (UT)). A few months after operations began, the observing schedule was extended 30 min, allowing GOLD to observe the western coast of South America just after sunset. At later LTs GOLD suspends observations for instrument safety. Near midnight, the Sun, which is too bright for GOLD to safely observe, becomes visible in the sky behind the Earth. The most significant change to the

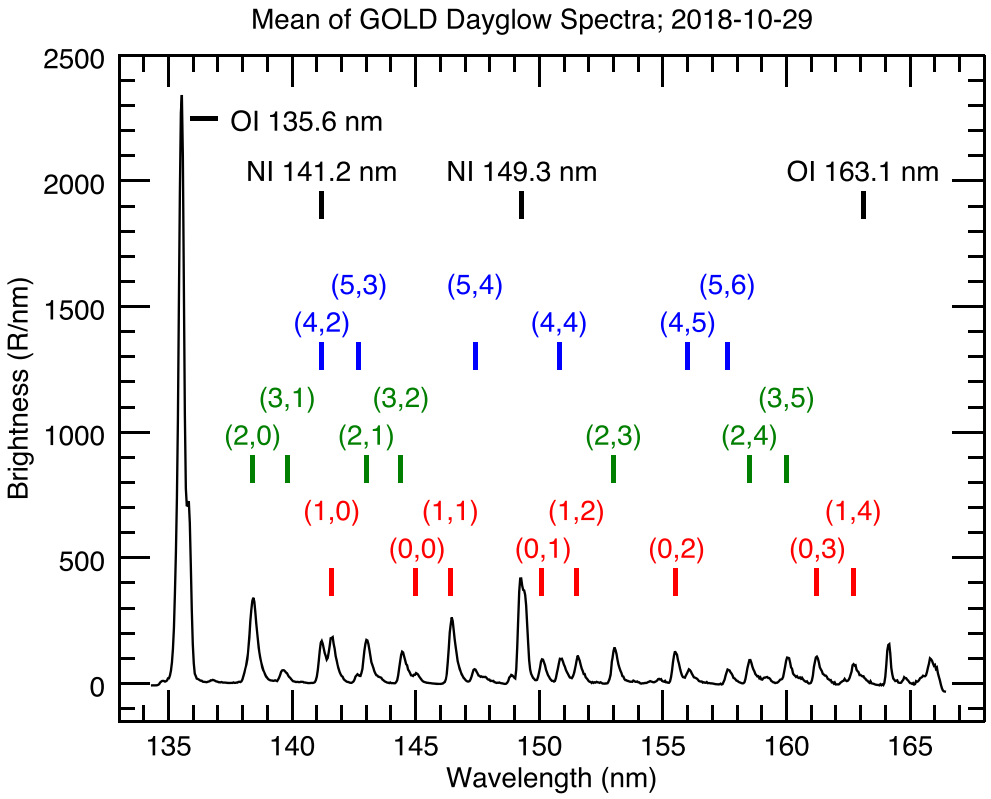

Figure 1. Mean of 11,157 observed spectra from 29 October 2018 where the solar zenith angle and emission zenith angle were both less than 30°. The resolution and sensitivity are consistent with preflight, laboratory measurements.

operations schedule was in March 2019 when it was recognized that gain decreased for the O I 135.6-nm emission more rapidly than expected in Channel B. Gain changes proportional to the total counts detected were anticipated and expected to be significant for the 135.6-nm line, which is an order of magnitude brighter than the other emissions observed. As the detector gain decreases, the charge generated by photoevents can fall below the preset threshold for detection. Since gain changes were anticipated, each channel includes a mechanism to rotate the grating slightly, moving the 135.6-nm line onto a more responsive region of the detector. The grating was rotated in March, and more recent Channel B observations have been primarily on the nightside where the emissions, and counts produced, are sufficiently low that gain changes that are negligible. This change in operations does not affect the science goals of the mission because Channel A can independently make all the required dayside measurement (summarized in Table 1) since sensitivity losses during spacecraft integration were included when building GOLD, but the losses were insignificant.

Table 1
GOLD Science Requirements

Location	Requirement
Sunlit disk	
	Disk images of O 135.6 nm and N_2 LBH emissions over ±60° latitude and ±70° longitude relative to spacecraft nadir
	Disk images of thermospheric temperature at 60-min cadence, 250-km × 250-km spatial resolution (at nadir) and a precision of ±55 K
	Disk images of O/N_2 column density ratio at 30-min cadence, 250-km × 250-km spatial resolution (at nadir) and a precision of 10%
Night disk	
	Images of Nmax *F*2 at the peak of the equatorial arcs, a precision of 10%, and a latitude resolution of 2°
	Track ionospheric bubbles within an equatorial arc with a precision of 20% in brightness and 100-km spatial resolution (at nadir) in longitudinal direction
Limb	
	Exospheric temperature near equatorial with a precision of ±40 K from N_2 LBH emissions
	Molecular oxygen (O_2) column densities at vertical resolution of 10 km and precision of ±10% above 150 km from stellar occultations

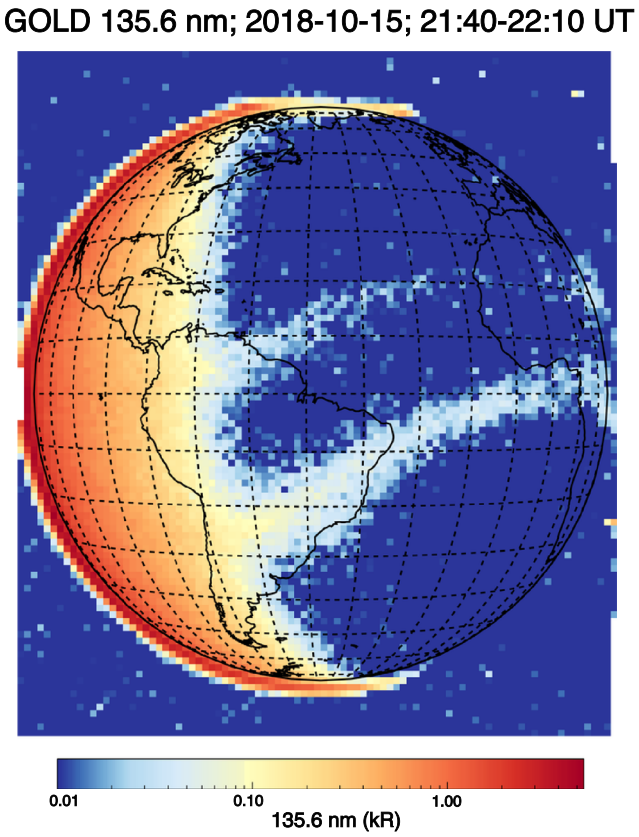

Figure 2. Observations at 135.6 nm on 15 October (Day 291) 2018 by Channel A at 21:40–22:10 UT (18:30–19:00 satellite LT). Observations are at 0.2 nm spectral resolution and gridded onto a constant angular (fixed geographic) grid with 125-km × 125-km spacing at nadir. The entire spectrum is observed simultaneously with the 135.6-nm emission, which is primarily from atomic oxygen (O). Emissions seen on the west (day) side are predominately dayglow. On the east (night) side, auroral emissions are evident at the highest latitudes and emissions from the crests of the EIA are seen near the equator.

Since October 2018, GOLD has made nearly continuous observations from 03:00 to 21:30 LT (06:10 to 00:40 UT). Data losses have been very infrequent. During 2019, only ~6 hr of data were lost, most for instrument resets (recovery from error detection and data correction (EDAC) events) and a small portion due to weather (the frequencies used for the downlink are susceptible). Temporary data losses due to errors during transmission from the ground station to the Laboratory for Atmospheric and Space Physics (LASP) also occur, but these have been recoverable by retransmission from the ground receiving station where data are retained for 6 days after transmission to LASP.

Within the 30-min period of a dayside full-disk scan, a channel observes the disk for 24 min and typically does a limb scan in the 6 min remaining. When a sufficiently bright ultraviolet (UV) star transits the limb, the time may instead be devoted to an occultation. At 17:00 LT Channel B begins partial-disk scans on the nightside disk at a 15-min cadence, alternating between north and south latitudes. Channel A continues making full-disk scans and limb observations until 20:00 LT. From 20:00 to 21:00 LT (to 21:30 LT since early 2019), both channels observe only the nightside disk, one at north and the other at south latitudes (limb observations are suspended during partial-disk scans). The following sections discuss the observations using the four modes described above.

3.1. Dayglow Observations

Dayside airglow observations are typically conducted as either full-disk or limb scans. Since the disk data products are retrieved from near-nadir observations, the information retrieved is weighted by the line-of-sight contributions, most of which come from approximately one scale height around the peak of the daytime airglow emission profile, which is near 160 km at most locations. Therefore, the disk emissions are indicative of conditions in the lower-middle thermosphere. The objective of the limb scans is to quantify how rapidly brightness decreases with altitude above the peak. This depends on the exospheric temperature.

3.1.1. Full-Disk Scans

The observations used to produce images of the temperature and composition ratio near 160 km in the thermosphere are made by scanning the full-disk between 06:10 and 20:10 UT. Each covers the viewable dayside and nightside. To produce a full-disk scan, separate scans of the north and south latitudes, starting above the limb in the east and ending above the limb in the west, are combined. The individual scans cover from above the poles to slightly beyond the geographic equator (overlapping at equator). While nightside emissions are observed in the full-disk scans, the signal-to-noise ratio (SNR) of the partial-disk scan mode is a factor of ~2 higher, as discussed below in section 3.3. During each half-hour, the dayside limb emission profile is also observed unless an occultation observation is scheduled. The limb and nightside disk scans are discussed in later sections. Dayside observations that do not cover the full disk, for example, using a fixed slit position, are "special" modes.

The spatial-spectral image cubes (L1C data) from the disk scans are placed on a fixed latitude-longitude grid containing the brightness as a function of wavelength observed at each location. The files also contain other information, including the original counts, uncertainties, and backgrounds. An example of the spectra (mean) within these cubes is shown in Figure 1. By summing the signals from specific emission features, full-disk images can be constructed like the one shown in Figure 2 of the 135.6-nm feature. While both O I 135.6-nm and an N_2 LBH band at 135.4 nm contribute to the feature, at the spectral resolution (~0.2 nm) being used for full-disk imaging, the LBH contribution is typically small, ~10–15%. Due to the limited LBH contribution to 135.6-nm feature, dramatic storm time changes in composition can be discerned using the L1C data as shown by Gan et al. (2020). The disk temperature (Tdisk) and oxygen to molecular

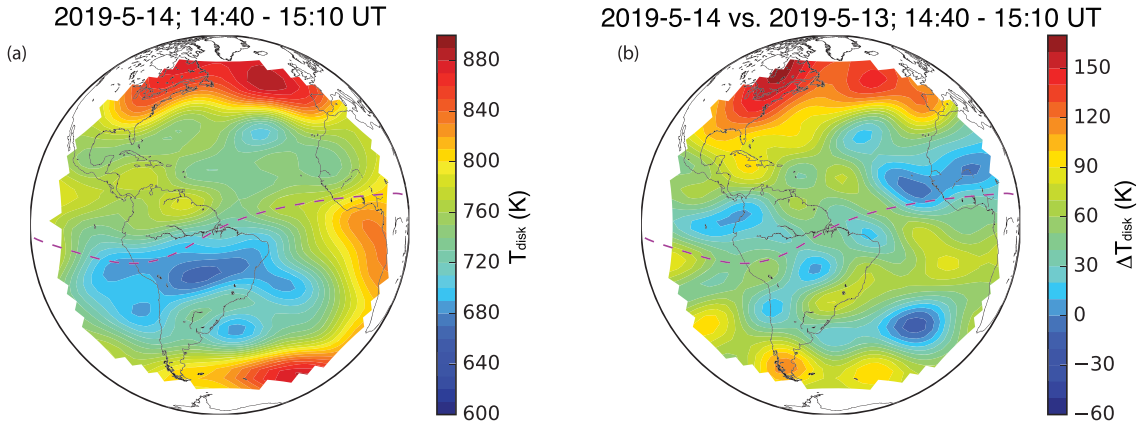

Figure 3. (a) Image of disk neutral temperature derived from GOLD day disk observations taken at 14:40–15:10 UT (11:30–12:00 satellite LT) on 14 May (Day 134) 2019. The highest temperatures are observed at the northern latitudes where the observations are nearer regions of auroral energy deposition. (b) Difference in disk temperatures (Tdisk) retrieved from GOLD observations at 14:40–15:10 UT on 14 May 2019 from previous day. Atmospheric temperature increases are evident at the higher latitudes in both hemispheres.

nitrogen density ratio ($\Sigma O/N_2$), both are Level 2 (L2) data products (i.e., those retrieved from the L1C data), provide a more complete context for such changes on the sunlit disk.

An example of the Tdisk values retrieved from observations made following a geomagnetic storm is shown in Figure 3a. These observations were made between 14:40 and 15:10 UT (11:30–12:00 LT at the satellite) on 14 May 2019 following a geomagnetic storm with *Kp* ~6 at 03:00–09:00 UT on 14 May. The difference between the temperatures on 14 May and those from the previous day is shown in Figure 3b. The Tdisk values shown were retrieved at 250-km × 250-km spatial resolution (nadir) from an image taken at a 30-min cadence. To better show the large-scale storm effects, spatial variations smaller than about 1,500 km are filtered out from the Tdisk and ΔTdisk observations. While the current publicly available Tdisk data are at 125-km × 125-km resolution, that is a factor of 2 finer spatially and temporally than originally planned (see Table 1). The 250-km × 250-km spatial resolution data product (summed) used in Figures 3a and 3b is in preparation for release. Although the 14 May 2019 storm is relatively small, a temperature increase at the higher latitudes is apparent. Having the temperatures in the same altitude region where the column densities are measured provides a significant, additional constraint when modeling the T-I system. The Tdisk data product has been presented by Evans et al. (2020) and will be the subject of a future paper.

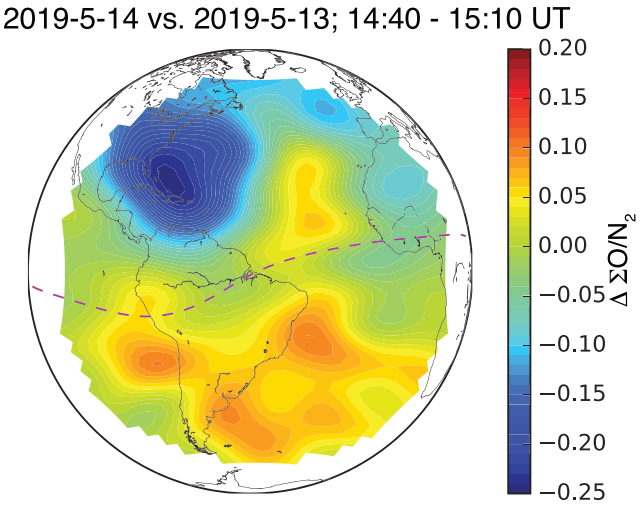

Figure 4. Difference in column density ratios ($\Delta\Sigma O/N_2$) retrieved from GOLD observations at 14:40–15:10 UT (11:30–12:00 satellite LT) on 14 May 2019 from previous day. The largest decrease occurs near the largest temperature increases in Figure 3b, but the morphology differs.

Geomagnetic storms also alter the neutral composition of the thermosphere. Changes observed in $\Sigma O/N_2$ ($\Delta\Sigma O/N_2$) during the same 14 May 2019 storm are shown in Figure 4. As for ΔTdisk, filtering has removed the spatial variations smaller than about 1,500 km. From comparison of Figures 3b and 4, it is evident that the disk temperatures exhibit distinct differences in structure from $\Sigma O/N_2$. But the most depleted $\Sigma O/N_2$ region in the Northern Hemisphere coincides with largest temperature increase. Further discussion of the $\Sigma O/N_2$ data product, the algorithm used to obtain it and the uncertainties have been presented by Correira et al. (2018).

While the preceding discussion has focused on geomagnetic storm effects, other geophysical influences can be identified. An example is the work of Oberheide et al. (2020) who found that a major sudden stratospheric warming event in the Northern Hemisphere induced an ~10% depletion in the zonal mean of $\Sigma O/N_2$.

3.1.2. Day Limb Scans

Dayglow limb emission profiles have been used for decades to deduce exospheric temperatures (e.g., Meier & Anderson, 1983); the GOLD mission

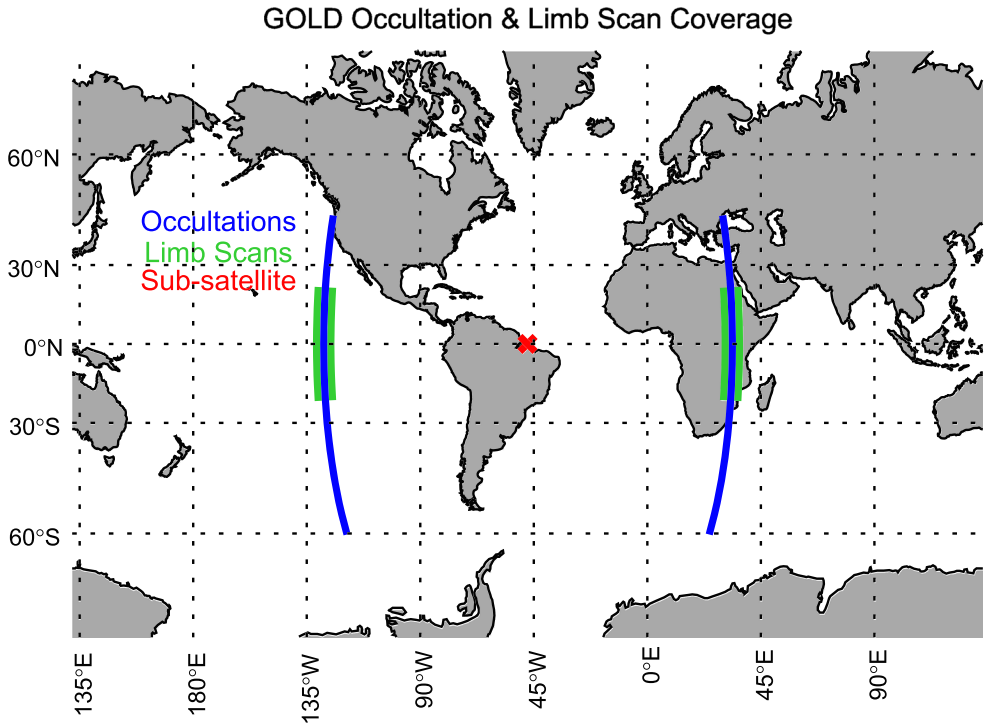

Figure 5. Locations of GOLD limb measurements. The green bars indicate the longitudes and latitude ranges where limb emission profile measurements are made. The blue curves mark the longitudes and latitudes encompassed by the occultation measurements.

also uses this technique. Temperatures are derived using only the N_2 LBH emission profile because recombination is known to increase the O I 135.6-nm emissions at high altitudes near the equator. A fundamental assumption of the technique, that the brightness variation with altitude be relatable to the neutral density variation with altitude, is thought to be valid for the LBH bands. The algorithm has been used and validated on previous missions, (Bougher et al., 2017; Christensen et al., 2003; Lo et al., 2015; Meier et al., 2015). A discussion of the implementation for GOLD, the retrieved data, and the associated uncertainties has been presented by Veibell et al. (2018).

During normal dayside observations (3:00–20:00 SLT), a limb scan of the (sunlit) dayside in each hemisphere is performed within every 30-min period unless an occultation is scheduled within that period. Since LT at the tangent locations change throughout the orbit, the eastern limb is scanned before local noon at the spacecraft; after that, the western limb is scanned. Since GOLD's longitude and latitude are fixed, the tangent points are also fixed. The longitudes and latitudes over which limb profiles are processed and exospheric temperatures retrieved are indicated by the green bars in Figure 5. The limb scans cover 486 km at the limb, covering tangent altitudes from −50 to 430 km at the equator. For each limb scan, north or south of the equator, limb profiles are extracted at 1.25° intervals between 15°N (S) latitude and 5°S (N) latitude. From the resulting sequence of observations, the exospheric temperature can be observed through 8 hr or more of LT at the tangent locations.

An example of the exospheric temperatures retrieved is shown in Figure 6. The limb profile at 3.4°N latitude and the fit to it are shown in Figure 7. The uncertainties in the retrieved values are consistent with the required precision, ±40 K.

3.2. Occultations

To quantify the O_2 densities in Earth's lower-middle thermosphere, GOLD uses stellar occultations. While O_2 is a major constituent of the lower thermosphere, as are O and N_2, it does not emit in the 134- to 162-nm wavelength range. However, it does absorb photons—in the Schumann-Runge continuum (e.g., Ogawa & Ogawa, 1975). This photoabsorption varies smoothly, decreasing by a factor of ~3 from 140 to

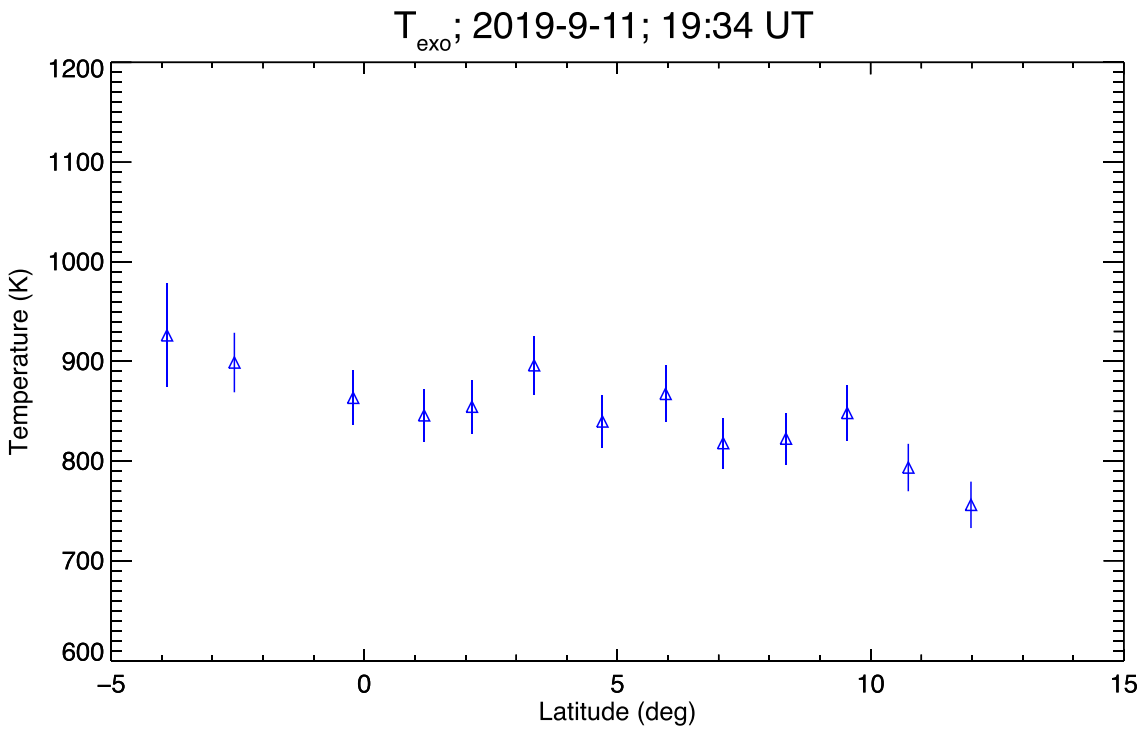

Figure 6. Exospheric temperatures derived from a N_2 limb scan of northern latitudes near the equator on 11 September (Day 254) 2019 at 19:34 UT (16:24 satellite LT). Error bars are $\pm 1\sigma$.

160 nm. When a sufficiently bright and stable UV star rises or sets through the thermosphere, the brightness changes depend on the absolute densities along the line of sight. If the observations extend to a sufficiently high altitude to be above significant photoabsorption, the O_2 density profile can be derived from the brightness changes.

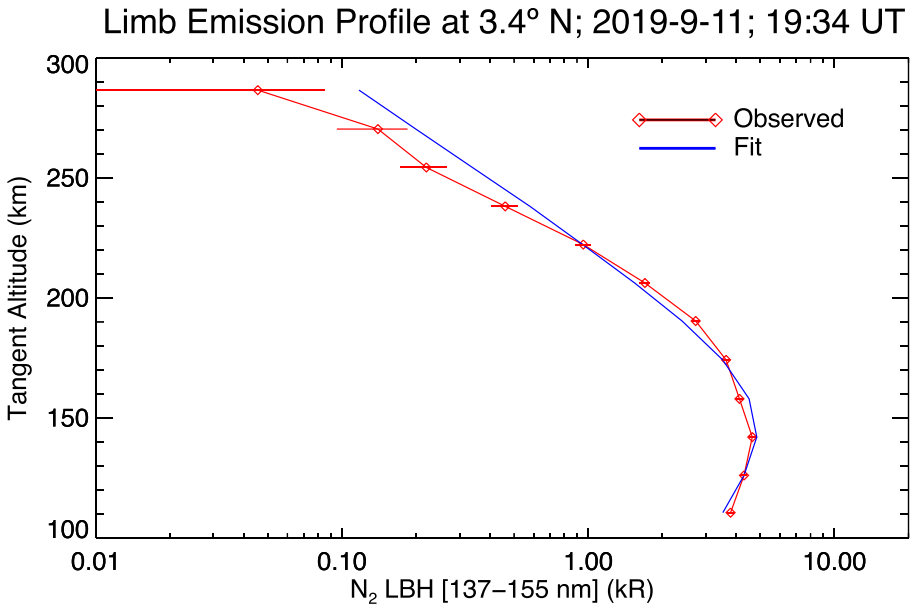

Figure 7. Observed limb emission profile (red) from 3.4° north latitude in Figure 6 and best fit model profile (blue). Error bars are $\pm 1\sigma$.

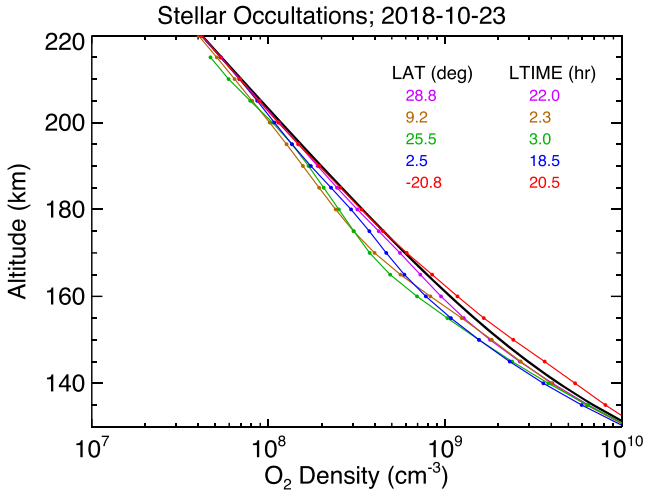

Figure 8. O_2 density profiles retrieved from stellar occultations on 23 October 2018. The latitude and local time (tangent point) for each profile are shown using the same color as the curve for the retrieved profile. The a priori profile (black, NRLMSISE-00) is also shown. Near 170 km, the retrieved densities are typically lower than those of the a priori profile.

From geostationary orbit, only stars near the ecliptic will rise and set through the Earth's atmosphere. Also, relatively bright and stable emission in the FUV is necessary for useful stellar occultation measurements, and bright Types O and B stars provide that. There are enough such stars near the ecliptic to provide good temporal and latitudinal coverage. While the number of opportunities varies daily—stars are not distributed uniformly—GOLD performs ~10 per day during most of the year. Since GOLD's location is fixed relative to the Earth, the geographic locations at which the occultations of a star occur (rising and setting) are also fixed. In Figure 5 the geographic latitudes and longitudes range over which the occultations are observed is marked by the blue curves.

The widest entrance slit in each channel allows observation of an occultation through an ~500-km range of tangent altitude without moving the slit. While a wide entrance slit is used, stellar images are much smaller than the slit width; consequently, the imaging performance dictates the spectral resolution for a star. Since dayside occultations also observe the dayside airglow, possibly producing higher count rates than can be accommodated by the 6 Mbps downlink, only data from an area adjacent to the star are downlinked. These adjacent areas are used to derive and subtract dayglow contributions. The nightside occultations of a star, absent such contributions, have better signal to noise.

An example of the O_2 density profiles retrieved from nightside occultations on a single day is shown in Figure 8. Lumpe et al. (2020) have described the occultations and retrieval of O_2 densities. The profiles retrieved for each of the five occultations (lines with diamonds) are compared with the retrieval a priori (smooth, black line) The GOLD O_2 algorithm uses a fixed a priori profile for all retrievals. This profile is a derived (from the Naval Research Laboratory Mass-Spectrometer-Incoherent-Scatter model, NRLMSISE-00, Picone et al., 2002) model run for solar minimum conditions. As discussed in Lumpe et al. (2020), the retrieval is tightly constrained toward the a priori at the highest (>200 km) and lowest (<130 km) altitudes, where the information content is low due to noise dominance (low O_2 densities) or complete absorption. Between 130 and 200 km, the O_2 density is of high quality with zero a priori bias. As shown in Figure 8, the retrieved densities are as much as a factor of 2 lower than the NRLMSISE-00 profile between 160 and 220 km. This difference is not atypical. The GOLD O_2 is generally lower (day or night) than NRLMSISE-00 predictions.

Differences between the observations and empirical model predictions in the lower and middle thermosphere are not surprising due to the limited amount of O_2 density data available, but the magnitude of the differences is. At the higher altitudes atomic oxygen is a dominant species, making O_2 density measurements especially challenging. Unfortunately, a reliable, independent source of densities for validation has not been identified. Further examination of thermospheric O_2 densities is clearly needed.

3.3. Nightglow Observations: Partial-Disk Scans

Outside the auroral regions, the most significant emission observed at night is O I 135.6 nm from the crests of the EIA. The ionospheric density on which its brightness depends has been of great interest for decades due to its variability and structure. Consequently, the O I 135.6-nm emission produced is also of significant interest.

While the emission from the EIA is typically an order of magnitude brighter than other nonauroral sources, it is an order of magnitude dimmer than the daytime airglow. The emission is produced by radiative recombination of atomic oxygen ions. Oxygen ions and electrons are produced on the dayside, prior to sunset. The eastward electric field from the ionospheric dynamo drives them across the magnetic field lines to higher altitudes. At higher altitudes the loss of atomic oxygen ions by charge exchange, which occurs rapidly with O_2 and N_2, is insignificant and significantly slower atomic loss processes are dominant. Gravitational forces also affect the flow, adding to the simultaneous, poleward flow of the ions. A result is enhanced ion concentrations, typically cresting near +15° and −15° geomagnetic latitude, that persist into the night.

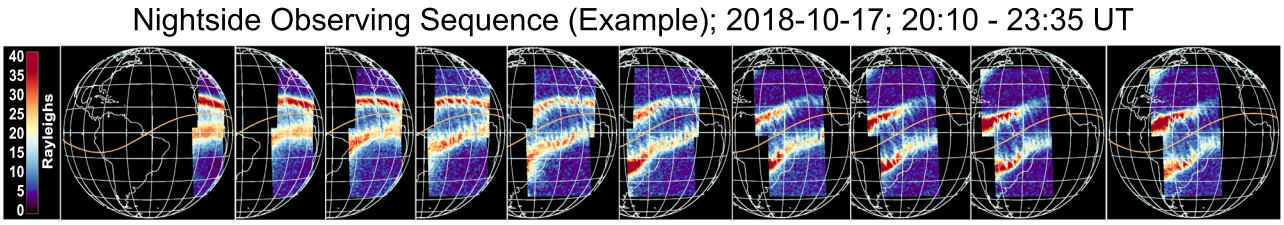

Figure 9. Typical sequence of nightside scans, example from 17 October 2018. The longitude ranges scanned in the Northern and Southern Hemispheres are selected to avoid locations illuminated by the Sun while observing near the terminator. Bubbles, seen most prominently on the equatorward edges of the EIA crests, are typical near equinox.

The partial-disk scan mode is designed to provide better SNR on the nightside than the full-disk scans. Three changes are made from the full-disk scans. First, the wider, low-resolution slit is used. This doubles the instrument's response to the Earth's emissions. Second, the observing time at each location is more than doubled by scanning only ~45° of longitude (near sunset for most scans) while maintaining a cadence of 15 min per scan. Third, the nighttime disk observations are not interrupted for limb scans or occultations. These changes increase the SNR by approximately a factor of 2 from that obtained when performing the full-disk scans discussed in section 3.1.1.

Each day at 18:00 LT (20:10 UT), Channel B begins partial-disk scans of the nightside, alternating between the Northern and Southern Hemispheres at a 30-min cadence. From 23:10 to 00:40 UT, Channel A scans the Northern Hemisphere on the nightside, while Channel B scans the Southern Hemisphere, increasing the cadence to 15 min. All the nightside, partial-disk scans (NI1 data) are binned onto a constant angular grid with ~93-km spatial resolution at nadir.

As noted earlier, the O I 135.6-nm emission from the EIA is produced by recombination of atomic oxygen ions, O^+, which can recombine directly with electrons or return to neutral oxygen through ion-ion mutual neutralization ($O^- + O^+$). While both processes produce O I 135.6-nm emission at all LTs, it is most prominent in the nightside EIA, and GOLD uses these nightside emissions for remote sensing of the EIA. The emissions reflect the climatology of the nightside EIA which depends on geomagnetic activity and thermospheric neutral winds in addition to the night-to-night variability produced by factors such as composition changes in the neutral atmosphere (e.g., Goncharenko et al., 2010; Immel et al., 2009) or disturbances of the neutral atmosphere (e.g., Makela & Otsuka, 2012). The GOLD mission observes especially interesting longitudes, over South America and the Atlantic, where the geomagnetic and geographic equators have their widest separation. While earlier observations (e.g., Liu et al., 2007; Luan et al., 2015) provided climatological descriptions, high cadence, synoptic views have rarely been available before GOLD. The IMAGE mission was able to capture broader morphology for multiple hours when its apogee was at low latitude but only in the Northern Hemisphere (Immel et al., 2006). Ground-based observations can provide high temporal coverage, but their spatial coverage is physically limited.

Shown in Figure 9 is a typical sequence of nightside images. Initially, only Channel B observes the nightside and at 20:00 LT, Channel A begins scanning the northern latitudes and B only the southern, increasing the cadence of images from 30 to 15 min. The equatorial anomaly, in which gaps—sometime referred to as bubbles—in the emission can be seen, is clearly identifiable. Some of the interesting and unexpected observations that occurred early in the mission, October–December 2018, have been discussed by Eastes et al. (2019). Dramatic changes in the location of the EIA are sometimes seen, with the separation between the crests doubling or the crests merging at the equator. Such changes have been seen even during quiet geomagnetic conditions. Further analysis of nightside observations has been presented by Cai et al. (2019). Another unexplained phenomenon that has occasionally been seen in the GOLD images is patches of O I 135.6-nm emission at midlatitudes (e.g., over Arecibo) for a brief period after sunset. Based on the initial studies of GOLD images, there are numerous phenomenon worthy of further study.

3.4. Other Observations and Modes

Although almost all the observations to date have been in one of the four modes described in previous sections, the operational flexibility of the instrument allows others. These have typically been referred to as

special modes. An example of data collected using a special mode of operation to improve the SNR for a specific objective is the gravity waves observations reported by England et al. (2020). Analyses of the current observations have also prompted the use of a modified version of the nightside scans used for observing each evening for early morning observations of the disk. The EIA in the morning is typically an order of magnitude dimmer than in the evening, but sums of full-disk data indicated the occasional presence of localized emissions. Some examples and analysis of those data have been presented by Laskar et al. (2020). A special mode that could also provide additional insights is the conjugate photoelectron excitation sometimes seen near the terminator on the nightside (Solomon et al., 2020). Alternate modes of observation continue to evolve and some may become part of the standard operations.

4. Conclusions

The GOLD mission provides simultaneous, synoptic images of composition and temperature across a hemisphere repeatedly throughout each day. GOLD's observations of the thermosphere and ionosphere are the first with global-scale spatial coverage and near-continuous temporal coverage. Given that previous measurements of $\Delta\Sigma O/N_2$ from low Earth orbit (LEO) have proven invaluable in advancing our understanding of the T-I system (e.g., TIMED/GUVI), GOLD data have the potential to provide a major next step in understanding the T-I system and advancing global T-I general circulation models.

Initial analyses of data from the GOLD mission have already provided new insights into the behavior of the thermosphere and ionosphere, and initial results from validation efforts indicate that the instrument is performing nominally and providing valid measurements. While the instrument operations and data processing are still being refined, the observations are already advancing the current understanding of the T-I system. This suggests that GOLD's combination of perspective, cadence, and geophysical data will continue to expand our understanding of the TI system.

Data Availability Statement

GOLD L1C and L2 data presented in this paper can be accessed at the GOLD Science Data Center (http://gold.cs.ucf.edu/search/) and at NASA's Space Physics Data Facility (https://spdf.gsfc.nasa.gov).

Acknowledgments
The authors thank the hundreds of people who had a role in the GOLD mission, including those at SES, Airbus, Arianespace, ESA, CNES, CSG, NASA HQ, NASA GSFC, CPI, CU/LASP, UCB/SSL, and UCF, and those who served on the many review panels. This research is supported by NASA Contract 80GSFC18C0061 to the University of Colorado.

References

Aryal, S., Tong, D., Jiuhou, L., Huixin, L., Geonhwa, J., Wenbin, W., et al., & the GOLD Science team (2019). Perturbation of the ionosphere-thermosphere system due to the July 2, 2019 total solar eclipse as observed by the Global-Scale Observations of the Limb and Disk (GOLD) mission, Abstract **SH43A-04** presented at **2019 AGU** Fall Meeting, San Francisco, CA, 9–13 Dec.

Bougher, S. W., Roeten, K. J., Olsen, K., Mahaffy, P. R., Benna, M., Elrod, M., et al. (2017). The structure and variability of Mars dayside thermosphere from MAVEN NGIMS and IUVS measurements: Seasonal and solar activity trends in scale heights and temperatures. *Journal of Geophysical Research: Space Physics*, *122*, 1296–1313. https://doi.org/10.1002/2016JA023454

Cai, X., Burns, A., Wang, W., Coster, A., Qian, L., Liu, J., et al. (2019), Comparison of GOLD nighttime measurements of OI 135.6 nm radiance with the total electron content map: Preliminary results, Abstract SA13B-3261 presented at 2019 AGU Fall Meeting, San Francisco, CA, 9–13 Dec.

Christensen, A. B., Paxton, L. J., Avery, S., Craven, J., Crowley, G., Humm, D. C., et al. (2003). Initial observations with the Global Ultraviolet Imager (GUVI) in the NASA TIMED satellite mission. *Journal of Geophysical Research*, *108*(A12), 1451. https://doi.org/10.1029/2003JA009918

Correira, J, Evans, J. S., Krywonos, A., Lumpe, J. D., Codrescu, M., Veibell, V., et al. (2018). Global-scale Observations of Limb and Disk (GOLD): Overview of O/N_2 and QEV science data products. Abstract SA21A-3169 presented at 2018 AGU Fall Meeting, Washington, DC. 10–14 Dec.

Eastes, R. W., McClintock, W. E., Burns, A. G., Anderson, D. N., Andersson, L., Codrescu, M., et al. (2017). The Global-scale Observations of the Limb and Disk (GOLD) mission. *Space Science Reviews*, *212*(1-2), 383–408. https://doi.org/10.1007/s11214-017-0392-2

Eastes, R. W., Solomon, S. C., Daniell, R. E., Anderson, D. N., Burns, A. G., England, S. L., et al. (2019). Global-scale observations of the equatorial ionization anomaly. *Geophysical Research Letters*, *46*, 9318–9326. https://doi.org/10.1029/2019GL084199

England, S. L., Greer, K. R., Solomon, S. C., Eastes, R. W., McClintock, W. E., & Burns, A. G. (2020). Observation of thermospheric gravity waves in the southern hemisphere with GOLD. *Journal of Geophysical Research: Space Physics*, e2019JA027405. https://doi.org/10.1029/2019JA027405

Evans, J. S., Lumpe, J., J., Correira, J., Viebell, V., Kyrwonos, A., Solomon, S. C., & Eastes, R. W. (2020). Neutral exospheric temperatures from the Global-scale Observations of the Limb and Disk (GOLD) mission. *Journal of Geophysical Research: Space Physics*, e2020JA027814. https://doi.org/10.1029/2020JA027814

Gan, Q., Eastes, R., Burns, A. G., Wang, W. B., Qian, L. Y., Solomon, S. C., et al. (2020). First synoptic observations of geomagnetic storm effects on the global scale OI 135.6nm dayglow in the thermosphere by the Global-scale Observations of the Limb and Disk (GOLD) mission. *Geophysical Research Letters*, e2019GL085400. https://doi.org/10.1029/2019GL085400

Goncharenko, L. P., Chau, J. L., Liu, H.-L., & Coster, A. J. (2010). Unexpected connections between the stratosphere and ionosphere. *Geophysical Research Letters*, *37*, L10101. https://doi.org/10.1029/2010GL043125

Immel, T. J., England, S. L., Zhang, X., Forbes, J. M., & DeMajistre, R. (2009). Upward propagating tidal effects across the E- and F-regions of the ionosphere. *Earth, Planets and Space*, *61*(4), 505–512. https://doi.org/10.1186/BF03353167

Immel, T. J., Sagawa, E., England, S. L., Henderson, S. B., Hagan, M. E., Mende, S. B., et al. (2006). Control of equatorial ionospheric morphology by atmospheric tides. *Geophysical Research Letters*, *33*, L15108. https://doi.org/10.1029/2006GL026161

Laskar, F. I., Eastes, R. W., Martinis, C. R., Daniell, R. E., Pedatella, N. M., Burns, A. G., et al. (2020). Early Morning Equatorial Ionization Anomaly from GOLD Observations. *Journal of Geophysical Research: Space Physics*, *125*, e2019JA027487. https://doi.org10.1029/2019JA027487

Liu, H., Stolle, C., Förster, M., & Watanabe, S. (2007). Solar activity dependence of the electron density at 400 km at equatorial and low latitudes observed by CHAMP. *Journal of Geophysical Research*, *112*, A11311. https://doi.org/10.1029/2007JA012616

Lo, D. Y., Yelle, R. V., Schneider, N. M., Jain, S. K., Stewart, A. I. F., England, S. L., et al. (2015). Nonmigrating tides in the Martian atmosphere as observed by MAVEN IUVS. *Geophysical Research Letters*, *42*, 9057–9063. https://doi.org/10.1002/2015GL066268

Luan, X., Wang, P., Dou, X., & Liu, Y. C.-M. (2015). Interhemispheric asymmetry of the equatorial ionization anomaly in solstices observed by COSMIC during 2007-2012. *Journal of Geophysical Research: Space Physics*, *120*, 3059–3073. https://doi.org/10.1002/2014JA020820

Lumpe, J., McClintock, W., Evans, J. S., Correira, J., Veibell, V., Beland, S., & Eastes, R. (2020). GOLD O_2: Algorithm and data product description. *Journal of Geophysical Research: Space Physics*, *125*, e2020JA027812. https://doi.org/10.1029/2020JA027812

Makela, J. J., & Otsuka, Y. (2012). Overview of nighttime ionospheric instabilities at low- and mid-latitudes: Coupling aspects resulting in structuring at the mesoscale. *Space Science Reviews*, *168*(1-4), 419–440. https://doi.org/10.1007/s11214-011-9816-6

Meier, R. R., & Anderson, D. E. Jr. (1983). Determination of atmospheric composition and temperature from the UV airglow. *Planetary and Space Science*, *31*(9), 967.

Meier, R. R., Picone, J. M., Drob, D., Bishop, J., Emmert, J. T., Lean, J. L., et al. (2015). Remote sensing of Earth's limb by TIMED/GUVI: Retrieval of thermospheric composition and temperature. *Earth and Space Science*, *2*(1), 1–37. https://doi.org/10.1002/2014EA000035

Oberheide, J., Pedatella, N. M., Gan, Q., Kumari, K., Burns, A. G., & Eastes, R. (2020). Thermospheric composition O/N_2 response to an altered meridional mean circulation during sudden stratospheric warmings observed by GOLD. *Geophysical Research Letters*, *47*, e2019GL086313. https://doi.org/10.1029/2019GL086313

Ogawa, S., & Ogawa, M. (1975). Absorption cross sections of $O_2(a^1\Delta_g)$ and $O_2(X^3\Sigma_g^-)$ in the region from 1087 to 1700 Å. *Canadian Journal of Physics*, *53*(19), 1845–1852. https://doi.org/10.1139/p75-236

Picone, J. M., Hedin, A. E., Drob, D. P., & Aikin, A. C. (2002). NRLMSISE-00 empirical model of the atmosphere: Statistical comparisons and scientific issues. *Journal of Geophysical Research*, *107*(A12), 1468. https://doi.org/10.1029/2002JA009430

Solomon, S. C., Andersson, L., Burns, A. G., Eastes, R. W., Martinis, C., McClintock, W. E., & Richmond, A. D. (2020). Global-scale observations and modeling of far-ultraviolet airglow during twilight. *Journal of Geophysical Research: Space Physics*, *125*, e2019JA027645. https://doi.org/10.1029/2019JA027645

Veibell, V., Evans, J. S., Lumpe, J. D., Correira, J., Eastes, R., Burns, A. G., et al., & GOLD Science Team (2018). Global-scale Observations of the Limb and Disk (GOLD): Overview of daytime exospheric temperature science data product. *Abstract SA21A-3171 presented at 2018 AGU Fall Meeting*, Washington, DC.